



# Mannose-coated superparamagnetic iron oxide nanozyme for preventing postoperative cognitive dysfunction



Qianyun Zhu<sup>a,1</sup>, Yuting Huang<sup>a,1</sup>, Xiaoling Zhu<sup>a</sup>, Lijun Peng<sup>a</sup>, Huan Wang<sup>a</sup>, Shan Gao<sup>b</sup>, Zhilai Yang<sup>a,\*\*\*</sup>, Jiqian Zhang<sup>a,\*\*</sup>, Xuesheng Liu<sup>a,\*</sup>

<sup>a</sup> Department of Anesthesiology, The First Affiliated Hospital of Anhui Medical University, Key Laboratory of Anesthesiology and Perioperative Medicine of Anhui Higher Education Institutes, Anhui Medical University, Hefei, PR China

<sup>b</sup> Department of Pharmacology, Basic Medical College, Anhui Medical University, Hefei, PR China

## ARTICLE INFO

### Keywords:

Nanoparticles  
Postoperative cognitive dysfunction  
Neuroinflammation  
Reactive oxygen species

## ABSTRACT

Postoperative cognitive dysfunction (POCD) is associated with increased postoperative morbidity and mortality in patients. Excessive production of reactive oxygen species (ROS) and the consequent inflammatory response in the postoperative brain play crucial roles in the development of POCD. However, effective ways to prevent POCD have yet to be developed. Moreover, effective penetration of the blood-brain barrier (BBB) and maintaining viability *in vivo* are major challenges for preventing POCD using traditional ROS scavengers. Herein, mannose-coated superparamagnetic iron oxide nanoparticles (mSPIONs) were synthesized by co-precipitation method. The BBB penetration of mSPIONs was verified through fluorescent imaging and ICP-MS quantification. The ROS scavenging and anti-inflammatory of mSPIONs were evaluated in H<sub>2</sub>O<sub>2</sub>-treated J774A.1 cells and in tibial fracture mice model. The novel object recognition (NOR) and trace-fear conditioning (TFC) were used to test the cognitive function of postoperative mice. The average diameter of mSPIONs was approximately 11 nm. mSPIONs significantly reduced ROS levels in H<sub>2</sub>O<sub>2</sub>-treated cells and in hippocampus of surgical mice. mSPIONs administration reduced the levels of IL-1 $\beta$  and TNF- $\alpha$  in the hippocampus and inhibited surgery-upregulated HIF1- $\alpha$ /NF- $\kappa$ B signaling pathway. Moreover, mSPIONs significantly improved the cognitive function of postoperative mice. This study provides a new approach for preventing POCD using a nanozyme.

## 1. Introduction

Postoperative cognitive dysfunction (POCD) is a common postoperative complication characterized by cognitive dysfunction, such as memory loss, inattention, a decline in information handling, and cognitive flexibility [1]. It can persist for days, months, and may deteriorate further, which decreases the quality of life and increases a heavy financial burden on society and health care system [2,3]. However, to this day, there is no satisfactory approach to prevent POCD.

Although the pathogenesis of POCD is currently unclear, accumulated evidences indicate that oxidative stress and neuroinflammation are key

mechanisms in POCD development [4,5]. Surgical trauma activates microglia in the central nervous system (CNS), contributing to increased reactive oxygen species (ROS) production which results in neuroinflammation [6,7]. Thus, scavenging ROS in the CNS may be a target for the treatment of POCD. However, the application of traditional exogenous ROS scavenger has some limitations. Firstly, they face challenges such as poor stability, pH sensitivity, and high cost [8]. Secondly, they have difficulty in penetrating the blood-brain barrier (BBB) [9]. Despite the disrupt BBB integrity in postoperative brain [10,11], a slight or no increase in permeability to small therapeutic molecules (<1000 Da) was observed [12], thus their neuroprotective effects are still limited.

\* Corresponding author. Department of Anesthesiology, the First Affiliated Hospital of Anhui Medical University, Key Laboratory of Anesthesiology and Perioperative Medicine of Anhui Higher Education Institutes, Anhui Medical University, No. 218 Jixi Road, Hefei, 230022, Anhui Province, PR China.

\*\* Corresponding author. Department of Anesthesiology, the First Affiliated Hospital of Anhui Medical University, Key Laboratory of Anesthesiology and Perioperative Medicine of Anhui Higher Education Institutes, Anhui Medical University, No. 218 Jixi Road, Hefei, 230022, Anhui Province, PR China.

\*\*\* Corresponding author. Department of Anesthesiology, the First Affiliated Hospital of Anhui Medical University, Key Laboratory of Anesthesiology and Perioperative Medicine of Anhui Higher Education Institutes, Anhui Medical University, No. 218 Jixi Road, Hefei, 230022, Anhui Province, PR China.

E-mail addresses: [yangzhilai@163.com](mailto:yangzhilai@163.com) (Z. Yang), [jiqianzh@mail.ustc.edu.cn](mailto:jiqianzh@mail.ustc.edu.cn) (J. Zhang), [liuxuesheng@ahmu.edu.cn](mailto:liuxuesheng@ahmu.edu.cn) (X. Liu).

<sup>1</sup> Co-first author: Qianyun Zhu and Yuting Huang contributed equally to this work.

Moreover, the slow opening of the damaged BBB takes several hours, resulting in a low accumulation of drugs in the postoperative brain during the early period of oxidative damage. Therefore, it is imperative to identify new ROS scavengers that can effectively cross the BBB to prevent POCD.

Over the past two decades, nanoparticles have been explored as potential candidates for the treatment of various diseases [13]. Benefiting from the advances in nanotechnology and nanoscience, antioxidant strategies based on multifunctional nanomaterials have been widely investigated. Thereinto, nanozymes, a new generation of enzyme mimics, have recently attracted considerable attention. Nanozymes are nanomaterials with enzymatic catalytic properties [14], and are classified primarily into the oxidoreductase and hydrolase families [15]. Iron oxide nanoparticles (IONPs) are one of promising nanozymes [16,17]. Under acidic conditions, IONPs present peroxidase-like properties to catalyze  $H_2O_2$  breakdown to a highly toxic hydroxyl radical. In parallel, they exhibit catalase (CAT)-like activity to decompose  $H_2O_2$  into oxygen and water under neutral physiological conditions [18]. In the CNS, IONPs are favorable due to their CAT-like activity and antioxidant effects. Zhang et al. found that dietary IONPs scavenged ROS by catalyzing intercellular  $H_2O_2$  breakdown through their CAT-like activity and ameliorate neurodegeneration in *Drosophila* [19]. In an ischemic stroke model, IONPs drove intrinsic ROS scavenging and inflammation-suppressing properties and achieved favorable neuroprotective effects [20,21]. Despite these studies, the application of nanozymes, such as IONPs, for the prevention of POCD has not been reported. Here, we synthesized mannose-coated superparamagnetic iron oxide nanoparticles (mSPIONs) with a diameter of approximately 11 nm. As mannose can improve the BBB penetration of modified drugs [22], mSPIONs significantly reduced ROS levels in the postoperative mouse hippocampus. Consequently, mSPIONs administration reduced the levels of inflammation in the hippocampus and significantly improved the cognitive function in postoperative mice. Additionally, inhibition of the surgery-upregulated HIF1- $\alpha$ /NF- $\kappa$ B

signaling pathway by mSPIONs may be involved in the alleviation of neuroinflammation. These results suggest a new approach for preventing POCD using nanozymes (Fig. 1).

## 2. Materials and methods

### 2.1. Synthesis and characterization of mannose-coated SPIONs (mSPIONs)

The SPIONs and mSPIONs were synthesized as described by Quang et al. via a co-precipitation method, with slight modifications [23]. Briefly, SPIONs were synthesized by combining  $FeCl_3 \cdot 6H_2O$  (6.02 mmol) and  $FeCl_2 \cdot 4H_2O$  (3.01 mmol) in 35 ml deoxygenated water at a molar ratio Fe (III)/Fe (II) of 2:1. An appropriate amount of  $NH_4OH$  was added to the black precipitate to a final pH of 10. The solution was centrifuged at 6000 rpm for 10 min, and the supernatant was discarded. Afterward, the precipitate was mixed with 10 ml of  $HNO_3$  (2 M) and 10 ml of  $Fe(NO_3)_3$  (0.35 M) and ultrasonicated for 1 h. The suspension obtained was added to a dialysis bag and dialyzed against 0.01 M  $HNO_3$  for 2 days in a sealed, oxidation-proof environment and stored at 4 °C. Finally, the product (10 ml) was mixed with 42  $\mu$ l of mannose (13.8 mol/L) and the pH was adjusted to 7 using  $NH_4OH$  to obtain mannose-coated SPIONs (mSPIONs) for characterization and testing.  $FeCl_3 \cdot 6H_2O$ ,  $FeCl_2 \cdot 4H_2O$ , and  $HNO_3$  were purchased from Shanghai Macklin Biochemical Co., Ltd (Shanghai, China).  $NH_4OH$  and  $Fe(NO_3)_3$  were purchased from Sigma-Aldrich (St. Louis, MO, USA).

The morphologies of the SPIONs and mSPIONs were characterized using transmission electron microscopy (TEM; JEM-2010, JEOL, Tokyo, Japan). The size distribution, the polydispersity index (PDI), and zeta potential of the SPIONs and mSPIONs were determined using dynamic light scattering (DLS; Zetasizer Nano ZS, Malvern Instruments Inc. Worcestershire, UK).

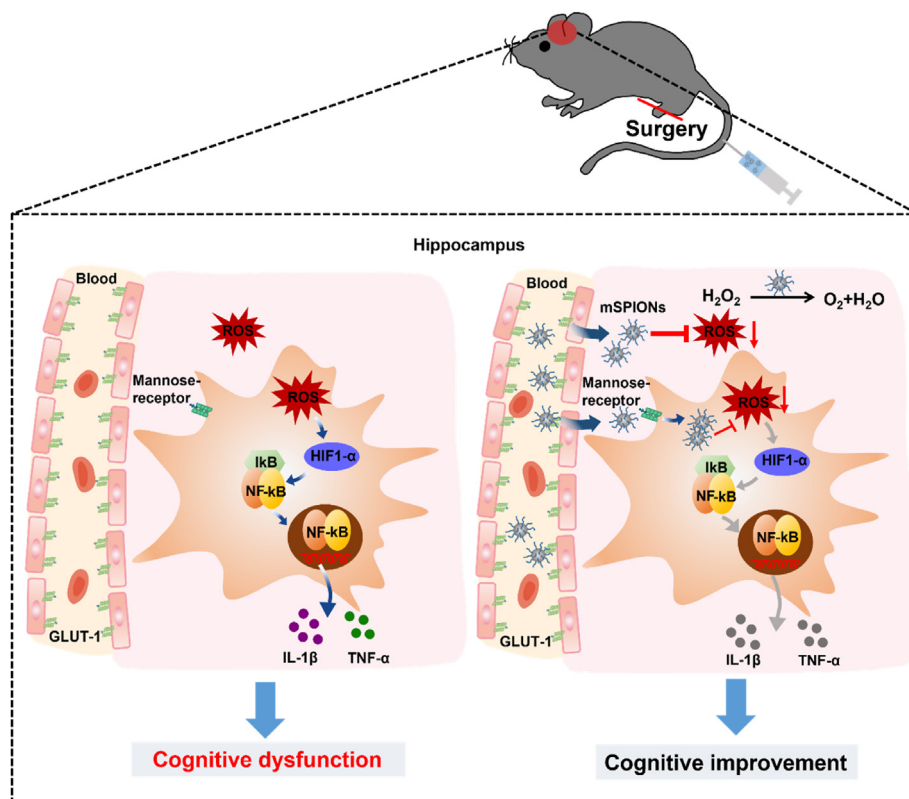


Fig. 1. Schematic diagram of mannose-coated superparamagnetic iron oxide nanoparticles (mSPIONs) for preventing postoperative cognitive dysfunction (POCD).

## 2.2. Catalase (CAT)-like activity of mSPIONs in vitro

To assess the CAT-like activity of SPIONs and mSPIONs to H<sub>2</sub>O<sub>2</sub>, 1 ml of H<sub>2</sub>O<sub>2</sub> (0.1 M) was incubated for 30 min in a 37 °C water bath with 50 µg/ml SPIONs and mSPIONs to monitor bubble generation. In addition, the ability of SPIONs and mSPIONs to scavenge H<sub>2</sub>O<sub>2</sub>-mediated free radical production was determined using terephthalic acid (TA) [24]. As a fluorescence probe, TA can capture hydroxyl radicals in a reaction system and generate highly fluorescent 2-hydroxy terephthalic acid. Briefly, 5 µl of TA (125 mM) and 0.5 ml of H<sub>2</sub>O<sub>2</sub> (0.5 mM) were mixed. Next, 50 µg/ml of SPIONs and mSPIONs were added to the mixture and incubated for 30 min at 37 °C in a water bath. Finally, the mean fluorescence intensity of the mixture was measured using a fluorescence microscope (Olympus IX71, Tokyo, Japan).

## 2.3. Cell culture

The mouse macrophage cell line (J774A.1), the mouse hippocampal neuronal cell line (HT22), and the mouse brain microvascular endothelial cell line (bEnd.3) were obtained from the China Center for Type Culture Collection (Wuhan, Hubei, China). Both types of cells were cultured in Dulbecco's modified Eagle's medium (DMEM; Hyclone, Logan, UT, USA) containing 10% (v/v) fetal bovine serum (FBS; FSD500, ExCell, Shanghai, China), penicillin (100 U/ml), and streptomycin (100 µg/ml) at 37 °C in a humidified atmosphere of 5% CO<sub>2</sub>.

## 2.4. Cell viability assay

The Cell Counting Kit-8 (CCK-8; BS350A, Biosharp, Hefei, China) was used to detect the cell viability of J774A.1 and HT22 cells in different conditions. After cellular fusion, 100 µl of the cell suspension was seeded into a 96-well plate at a density of  $1 \times 10^4$  cells/well, plastered overnight, and replaced with fresh medium containing different concentrations of SPIONs and mSPIONs (0, 10, 20, 50, 100, 200, and 400 µg/ml) for 24 h. In addition, the cells were treated with SPIONs and mSPIONs (50 µg/ml) for 12 h before exposure to H<sub>2</sub>O<sub>2</sub> (100 µM) for 100 min. Then, for another 1 h at 37 °C, 10 µl of CCK-8 solution was added into each well. Absorbance was measured at 450 nm using a microplate reader (Infinite M200 Pro, Tecan, Mannedorf, Switzerland).

## 2.5. Prussian blue staining of intracellular iron

Prussian blue staining was used to detect iron particles within J774A.1 cells. Cells were seeded on glass coverslips placed in 24-well plates at a density of  $5 \times 10^4$  cells/well and incubated for 12 h. Then SPIONs or mSPIONs (50 µg/ml) were then added into each well and incubated for 12 h. Before staining, cells treated with nanoparticles were washed three times with phosphate-buffered saline (PBS; Corning, NY, USA) and fixed in 4% paraformaldehyde (PFA; BL539A, Biosharp, Hefei, China) for 20 min. Cells were then stained with a Perls working solution containing equal amounts of potassium ferrocyanide and hydro-chloric acid (G1426, Solarbio, Beijing, China) for 30 min at 37 °C. The cells were washed with distilled water and observed under a microscope (Olympus IX71, Tokyo, Japan).

## 2.6. Intracellular H<sub>2</sub>O<sub>2</sub> measurement

J774A.1 cells were seeded in a confocal dish at a density of  $5 \times 10^4$  cells/dish and cultured in DMEM for 12 h. The cells were then treated with SPIONs or mSPIONs (50 µg/ml) for 12 h. The control group was treated with an equal volume of phosphate-buffered saline (PBS). After 12 h of incubation, cells were washed three times with PBS to clean up SPIONs or mSPIONs and treated with H<sub>2</sub>O<sub>2</sub> (100 µM) for 100 min in a CO<sub>2</sub> incubator at 37 °C. After washing twice with Dulbecco's PBS (DPBS), 5 µM of cell-permeable H<sub>2</sub>O<sub>2</sub>-probe peroxy orange 1 (PO1; SML0688; Sigma-Aldrich, St. Louis, MO, USA) prepared in DPBS was added to the

culture dishes and incubated for 30 min at 37 °C in the dark. The cells were then briefly washed with DPBS and immediately observed under a confocal laser microscope (LSM880, Carl Zeiss, Jena, Germany). The mean fluorescence intensity was analyzed using ImageJ software (National Institutes of Health, Bethesda, MA, USA).

## 2.7. Measurement of ROS production

ROS production induced by H<sub>2</sub>O<sub>2</sub> was measured by a ROS-detectable cell-permeable reagent 2',7'-dichlorodihydrofluorescein diacetate (DCFH-DA; S0033S, Beyotime, Shanghai, China). Briefly, J774A.1 cells were seeded in a confocal dish at a density of  $5 \times 10^4$  cells/dish and cultured in DMEM for 12 h. Cells were pretreated with SPIONs or mSPIONs (50 µg/ml) for 12 h and washed three times with PBS to remove extracellular SPIONs or mSPIONs before exposure to H<sub>2</sub>O<sub>2</sub> (100 µM) for an additional 100 min. The cells were incubated with DCFH-DA (10 µM) for 30 min at 37 °C. Subsequently, the residual agents were removed using PBS and replaced with 1 ml of DMEM without serum. Images were captured using a confocal microscope (LSM880, Carl Zeiss, Jena, Germany). The mean fluorescence intensity was analyzed using ImageJ software (National Institutes of Health, Bethesda, MA, USA).

To assess ROS generation in the CA1 region of the hippocampus after surgery, the redox-sensitive cell-permeable fluorophore dihydroethidium (DHE; D7008, Sigma-Aldrich, St. Louis, MO, USA) was used. The isolated brains were cut into 8-µm sections with a freezing microtome (MNT, SLEE, Mainz, Germany) and placed on microscope slides, followed by washing with PBS for 10 min. The samples were incubated with DHE (5 µM) in a light-protected humidified chamber at 37 °C for 30 min, and stained with DAPI after PBS washing. After washing with PBS, the samples were mounted using anti-fluorescence-quenching sealed tablets (Biosharp, Hefei, China). Fluorescence images were obtained using a fluorescence microscope (Olympus IX71, Tokyo, Japan). ImageJ software (National Institutes of Health, Bethesda, MA, USA) was used to quantify DHE fluorescence intensity in the brain sections.

## 2.8. Iron concentration measurements using inductively coupled plasma mass spectrometry (ICP-MS) in vitro and vivo

Before analysis, concentrated nitric acid was added to the cell samples and the whole brains at a ratio of 5:1, and fixed at 10 ml with distilled water. The Fe content was measured using ICP-MS (ELAN DRC II, PerkinElmer, Waltham, MA, USA).

## 2.9. Crossing the blood-brain barrier (BBB) model in vitro

The BBB model was established as previously reported [25]. bEnd.3 cells were plated on the upper chamber of 12-well culture inserts (0.4 mm pore size) (Corning, NY, USA) at a density of  $1 \times 10^5$  cells per/well, and the lower chamber was filled with 1.5 ml of DMEM. The growth medium was changed every 2 days. For determining the integrity of BBB model, transendothelial electrical resistance (TEER; World Precision Instruments, Inc. Sarasota, FL, USA) experiment was performed. The following experiment was performed only when TEER of the monolayer reached 200 Ω cm<sup>2</sup>. Additionally, J774A.1 cells were seed into another 12-well plates at a density of  $15 \times 10^4$  cells per/well. Cell culture inserts with bEnd.3 monolayers were then transferred to 12-well plates containing J774A.1 cells and co-cultured for 24 h. SPIONs or mSPIONs were added into the cell culture inserts at a final concentration of 50 µg/ml. After 8 h of incubation, J774A.1 cells on the plates were washed with PBS for three times, then trypsinized, and the Fe content in J774A.1 cells was analyzed by ICP-MS as described in section 2.8.

## 2.10. Crossing blood-brain barrier (BBB) in vivo

Healthy and postoperative mice (0, 1, 3, 7, and 14 days) were injected with 4 mg/kg of saline, fluorescein isothiocyanate (FITC)-labeled SPIONs

or mSPIONs through the tail vein to assess the content of SPIONs and mSPIONs crossing the BBB and the retention of mSPIONs in the post-operative brain. Brain tissues were obtained 24 h later, and ICP-MS was used to determine the Fe content in whole brains harvested from mice as described in section 2.8. The FITC fluorescence in the CA1 region of the hippocampus was measured using immunohistochemistry as described in section 2.16.

### 2.11. Animals

C57BL/6 male wild-type mice (6–8 weeks old) were purchased from the Shanghai SLAC Laboratory Animal Co., Ltd. (Shanghai, China). All mice were housed under a 12-h light–dark cycle at a constant room temperature and humidity, and allowed food and water ad libitum in accordance with the Guide for Care and Use of Laboratory Animals of the National Institutes of Health. All animal procedures were approved by the Ethics Committee of Anhui Medical University. All efforts were made to minimize the suffering of the mice.

### 2.12. Animal experimental protocol

Mice were randomly assigned to the following four groups: sham, mSPIONs, surgery, and surgery + mSPIONs. The mice were injected with saline or mSPIONs (4 mg/kg) through the tail vein and subjected to sham or surgery 6 hours later. For behavioral testing, the habituation, training, and testing phases of novel object recognition (NOR) were performed 1–3 days after surgery, respectively. A different cohort of mice was subjected to fear conditioning 1 day prior to surgery, and contextual tests 3 days after surgery. After 2 h of behavioral testing, the mice were euthanized, and brain tissue was harvested for subsequent experiments.

### 2.13. Surgical trauma

The experimental aseptic tibia fracture with intramedullary fixation model was established under general anesthesia, as previously described, with modifications to the anesthesia protocol [26]. Briefly, anesthesia was induced and maintained in a dedicated chamber with 3 vol% sevoflurane carried by 60% oxygen. After shaving and disinfecting the surgical area of the left hind paw, a longitudinal incision was made below the knee, and then the muscle was separated from the periosteum to expose the tibia. Afterward, a 0.38 mm pin was inserted into the tibial intramedullary canal, and osteotomy was performed to achieve intramedullary fixation. Next, the wound was irrigated and sutured using 5-0 Vicryl sutures. The mice were allowed to recover spontaneously from the anesthetic. The surgical procedure lasted about 10 min, and the total duration of general anesthesia was 20 min. Using a heating pad, body temperature was maintained at 36 °C–37.0 °C during surgery. To treat incision-related pain, buprenorphine (0.1 mg/kg) was administered after anesthetic induction and before skin incision. The mice in the sham group received the same anesthesia and analgesia.

### 2.14. Novel object recognition (NOR)

The NOR test was performed as described previously [4], with some modifications. This test consists of habituation phase, training phase, and testing phase. For the habituation phase (day 1), mice were placed in a chamber (50 cm × 50 cm × 40 cm) and allowed to adapt the context for 10 min without objects. During the training phase (day 2), the mice were placed in the same chamber, in which there were two identical objects (shape, size and color) placed in the opposite corners of the chamber, 10 cm from the side walls, and allowed to explore freely for 10 min 24 h after training (day 3), the mice were returned to the chamber, but one of the familiar objects was replaced by a novel object different in its shape, color, and texture. The testing phase lasted 10 min for each animal. All objects were previously tested to avoid biased preference. Each session was videoed from above and the behavior was monitored using the

Any-Maze software (Stoelting Co., Wood Dale, IL, USA). Object interaction was defined as the orientation of the nose to the object at less than 2 cm. The object discrimination index (DI) was calculated as: (time interacting with the novel object - time interacting with the familiar object)/(time interacting with the novel object + time interacting with the familiar object) × 100.

### 2.15. Trace-fear conditioning (TFC)

A different cohort of mice was used for the test. TFC was conducted as reported previously, which included a conditioning session 1 day before surgery and a contextual test session 3 days after surgery [27]. Briefly, animals were trained to associate a conditional stimulus (tone) with an aversive, unconditional stimulus (foot shock) in a conditioning chamber (Harvard Apparatus, Holliston, MA, USA). Specifically, an initial accommodation phase (120 s) was followed by six pairs of conditional stimuli (20 s auditory cue, 70 dB, 5 kHz) and unconditional stimuli (2 s foot shock, 0.70 mA) separated by a 25 s inter-pair interval. The pairs of conditional-unconditional stimuli were separated by random intervals of 45–60 s, with another 60 s remaining in the conditioning chamber. Surgery was then performed 24 h after the day of training. On post-operative day 3, the mice were returned to the same chamber for contextual assessment, without tone or shock stimuli, for 5 min. During training and testing, the changes in gravity of the mice on the deck were recorded as startle amplitude by Panlab Startle and Fear combined system with Packwin 2.0 software (Harvard Apparatus, Holliston, MA, USA). The recall of contextual fear memory was assessed by freezing behavior, defined as the complete lack of movement except for respiration.

### 2.16. Immunohistochemistry

The immunohistochemistry *in vitro* was performed by growing the cells on 14-mm round coverslips in 24-well dishes. Briefly, bEnd.3 or J774A.1 cells were plated on poly-L-lysine-treated coverslips and cultured for 12 h. After treatment with FITC-labeled mSPIONs (50 µg/ml) for 12 h, cells were washed with PBS, fixed with 4% PFA in PBS for 10 min, and then permeabilized with 0.1% Triton X-100 (BS084, Biosharp, Hefei, China). Then, cells were blocked with 2% bovine serum albumin (BSA; 4240, BioFroxx, Einhausen, Germany) in PBS at 37 °C for 1 h, and incubated with anti-GLUT-1 (1:100, ab115730, #Abcam, UK), anti-mannose-receptor (1:100, #ab1898, Abcam, UK) overnight at 4 °C. After washing in PBS for three times, cells were incubated with goat anti-rabbit Alexa Fluor 568 (1:200, #ab175471, Abcam, UK) for anti-GLUT-1 antibody and goat anti-mouse Alexa Fluor 568 (1:200, #ab175473, Abcam, UK) for anti-mannose-receptor antibody at 37 °C for 1 h. Finally, the nuclei of cells were stained by DAPI for 10 min at room temperature. After washing, images were captured using a fluorescence microscopy (Olympus IX71, Tokyo, Japan) with a 60 × oil objective. Image processing was performed with the ZEN software (Carl Zeiss, Jena, Germany).

For frozen section, mice were sacrificed under anesthesia and perfused transcardially with ice-cold PBS and then 4% PFA. Brains were removed, post-fixed in the same fixative for 24 h at 4 °C, and then cryoprotected in PBS containing 30% sucrose for a further 24 h. Brains were embedded in optimal cutting temperature (OCT) compound (Sakura, Japan) and immediately stored at –80 °C and then 8-µm coronal sections were cut using a freezing microtome (MNT, SLEE, Mainz, Germany) followed by mounting on adhesive slides. Sections were fixed with 4% PFA, washed with PBS, blocked for 1 h with 2% BSA in PBS containing 0.3% TritonX-100 (BS084, Biosharp, Hefei, China) at 37 °C, then incubated with a rabbit anti-iba-1 antibody (1:1000, #019-19741, Wako, Japan) at 4 °C overnight. After washing, the sections were incubated with goat anti-rabbit Alexa Fluor 568 (1:200, #ab175471, Abcam, UK) secondary antibody at 37 °C for 1 h in the dark and exposed to DAPI (BL105A, Biosharp, Hefei, China) in the dark at room temperature for 10

min. After washing, the sections were sealed on microscope slides with anti-fluorescence quenching sealed tablets (BL701A, Biosharp, Hefei, China). Images were acquired using a fluorescence microscopy (Olympus IX71, Tokyo, Japan) and processed using the ZEN software (Carl Zeiss, Jena, Germany).

### 2.17. Histologic examination

To investigate the toxicity of mSPIONs *in vivo*, mice were humanely sacrificed and the major organs (e.g., brain, heart, liver, spleen, lung, and kidney) were collected at the end of the experiment and then stained with hematoxylin and eosin (H&E) following the standard protocol. H&E-stained sections were visualized under a microscope (Olympus IX71, Tokyo, Japan).

### 2.18. Serum biochemical analysis

Peripheral blood was collected from mice 3 days after surgery. The concentrations of alanine transaminase (ATL), aspartate transaminase (AST), blood urea nitrogen (BUN), and creatinine (CR) in the serum were analyzed using an auto analyzer (Chemray 420, Rayto, Shenzhen, China).

### 2.19. Enzyme-linked immunosorbent assay (ELISA)

J774A.1 cells were seeded in 24-well plates at a density of  $10 \times 10^4$  cells/well and incubated for 12 h, followed by pre-treatment with mSPIONs (50  $\mu\text{g}/\text{ml}$ ) for 12 h, and then incubated with  $\text{H}_2\text{O}_2$  (100  $\mu\text{M}$ ) for 100 min in a 37 °C  $\text{CO}_2$  incubator. After treatment, the medium was collected, and 100  $\mu\text{l}$  of the medium was used for detection. The hippocampi extracted three days after surgery were homogenized in RIPA lysis buffer (BL504A, Biosharp, Hefei, China) and centrifuged at 12,000 rpm for 15 min at 4 °C to obtain supernatant for the assay. The concentrations of IL-1 $\beta$  and TNF- $\alpha$  in the hippocampus and medium were examined using ELISA kits (CSB-E08054 m, CSB-E04741 m, CUSABIO, Wuhan, China) according to the manufacturer's instructions. ELISA data were acquired using a microplate reader (Infinite M200 Pro, Tecan, Mannedorf, Switzerland) at 450 nm. Protein quantification was performed using a BCA Protein Assay Kit (BB-3401, Bestbio, Shanghai, China) according to the manufacturer's instructions.

### 2.20. Western blot analysis

Proteins were extracted from J774A.1 cells and hippocampi using RIPA lysis buffer (BL504A, Biosharp, Hefei, China) supplemented with phosphatase-protease cocktail inhibitor on ice, and then centrifuged at 12000 rpm for 15 min. The supernatant was collected and protein concentration was determined using the BCA Protein Assay Kit (BB-3401, Bestbio, Shanghai, China). The samples were denatured by heating at 95 °C for 15 min. Proteins from cells and lysed tissues were separated using 10% sodium dodecyl sulfate polyacrylamide gel electrophoresis (SDS-PAGE) and transferred to nitrocellulose membranes (Millipore, Bedford, MA, USA). To reduce background staining, the membranes were blocked for 1 h with 5% skim milk dissolved in Tirs-buffered saline containing 0.1% Tween-20 (TBST), then incubated with anti-HIF1- $\alpha$  (1:1000, #14179, Cell Signaling Technology, USA), anti-NF- $\kappa\text{B}$  p65 (1:1000, #8242, Cell Signaling Technology, USA), anti-phospho-NF- $\kappa\text{B}$  p65 (1:1000, #3033, Cell Signaling Technology, USA), and  $\beta$ -actin (1:1000, TA-09, ZSBIO, China) overnight at 4 °C, and subsequently washed with TBST. The bands were then incubated with the HRP-conjugated anti-rabbit and anti-mouse IgG (1:10000, #7074 and #7076, Cell Signaling Technology, USA) for 1 h at room temperature and washed. Afterward, the bands were then incubated with chemiluminescence (ECL) detection reagents (BL520A, Biosharp, Hefei, China) and visualized using a chemiluminescence instrument (Image Quant LAS 4000, GE Healthcare, Pittsburgh, PA, USA). Densitometric

analyses were performed using the ImageJ software (National Institutes of Health, Bethesda, MA, USA).

### 2.21. Statistical analysis

All sample sizes were chosen based on previous studies that used similar experimental paradigms. D'Agostino and Pearson tests or Shapiro–Wilk tests were used to examine the normal distribution of the data. F-tests were used to confirmed the equality variances of the data. The mean  $\pm$  SD is used to represent data with a normal distribution. The preferential interaction in the NOR test was analyzed using two-way analysis of variance (ANOVA) followed by the Šidák multiple comparisons test. Other data from multiple groups were analyzed using one-way ANOVA followed by Tukey's post hoc test. Significant differences were set at  $P < 0.05$ . Statistical analysis was performed using the GraphPad Prism software (version 8.0).

## 3. Results

### 3.1. Characterization of mSPIONs

SPIONs and mSPIONs were synthesized according to a previous method with modifications [23]. Transmission electron microscopy (TEM) images showed that both SPIONs and mSPIONs exhibited good shape (Fig. 2A and B). The average diameter of SPIONs and mSPIONs were  $10.56 \pm 2.33$  nm and  $11.42 \pm 1.65$  nm (Fig. 2C and D). The dynamic light scattering (DLS) analysis showed the hydrodynamic diameter of SPIONs and mSPIONs were  $124.37 \pm 4.90$  nm (PDI =  $0.28 \pm 0.04$ ) and  $123.27 \pm 1.89$  nm (PDI =  $0.21 \pm 0.01$ ) (Figs. S1A and B), and the zeta potential were  $-22.03 \pm 0.32$  mv and  $-18.67 \pm 0.43$  mv (Fig. S1C), respectively. Previous studies have reported that IONPs exhibit CAT-like activity under neutral conditions [20,21]. Similarly, we found co-incubation of SPIONs or mSPIONs with  $\text{H}_2\text{O}_2$  at 37 °C for 30 min resulted in many more bubbles than the control group, indicating that SPIONs and mSPIONs decomposed  $\text{H}_2\text{O}_2$  to generate oxygen (Fig. 2E). Furthermore, terephthalic acid (TA) was used to probe  $\text{H}_2\text{O}_2$  [24]. As shown in Fig. 2F and S1D, the mixture of TA and  $\text{H}_2\text{O}_2$  generated intense fluorescence, the mean fluorescence intensity was significantly reduced by SPIONs and mSPIONs, indicating that SPIONs and mSPIONs scavenge  $\text{H}_2\text{O}_2$  and possess catalase (CAT)-like activity *in vitro*.

### 3.2. mSPIONs reduce $\text{H}_2\text{O}_2$ -elevated cellular ROS levels

Next, cellular ROS scavenging by mSPIONs was assessed in J774A.1 cells. First, CCK-8 assays were used to evaluate cell viability after treatment with SPIONs or mSPIONs at various concentrations (0–400  $\mu\text{g}/\text{ml}$ ). The results showed that SPIONs and mSPIONs demonstrated similar cytotoxicity levels. SPIONs and mSPIONs at a concentration of 0–50  $\mu\text{g}/\text{ml}$  did not induce significant cytotoxicity after 24-h incubation (Figs. S2A and B). Therefore, 50  $\mu\text{g}/\text{ml}$  was used as the optimal concentration to study the effects of nanoparticles on J774A.1 cells. Furthermore, the cellular uptake of SPIONs and mSPIONs was tested using Prussian blue staining. We found that blue areatus iron granules were present in the cytoplasm of cells, the internalized particles were localized in a punctate manner, and the nuclei were counter-stained in red (Fig. 3A), indicating that SPIONs and mSPIONs could be phagocytosed by J774A.1 cells *in vitro*, which was mediated by mannose receptors (Fig. S3A). Moreover, the ROS scavenging activities of SPIONs and mSPIONs were assessed.  $\text{H}_2\text{O}_2$  is extensively used as an inducer of oxidative stress models. Specifically,  $\text{H}_2\text{O}_2$  can induced high levels of intracellular  $\text{H}_2\text{O}_2$ , which promotes ROS generation and induces oxidative stress; scavenging intracellular  $\text{H}_2\text{O}_2$  leads to a decrease in intracellular ROS [28]. The intercellular  $\text{H}_2\text{O}_2$  and ROS levels were measured using peroxy orange-1 (PO1) and 2',7'-dichlorodihydrofluorescein diacetate (DCFH-DA), respectively. The fluorescence results showed that cells exhibited

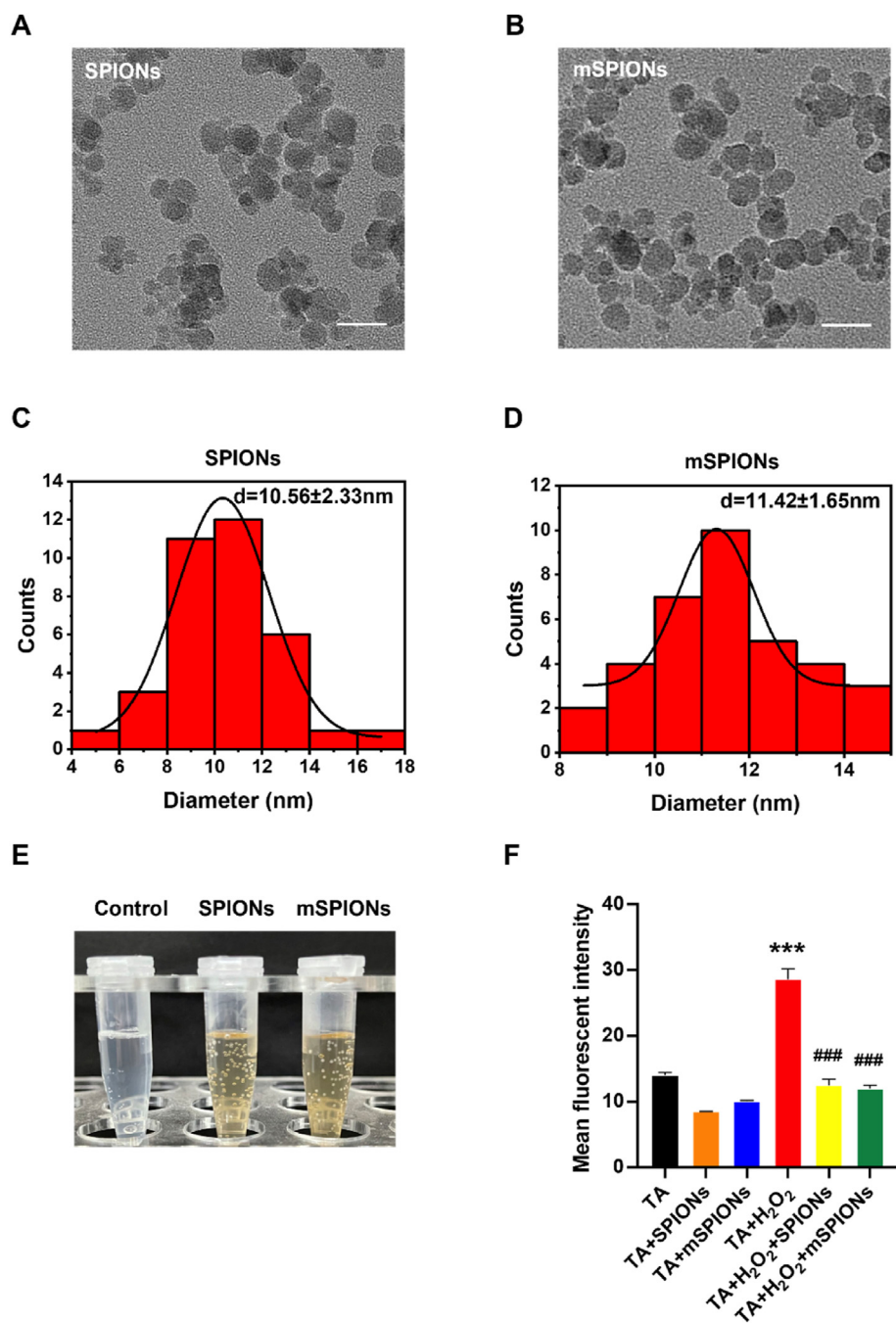


**Fig. 2.** Characterization of mannose-coated superparamagnetic iron oxide nanoparticles (mSPIONs). (A, B) Transmission electron microscopy (TEM) images of superparamagnetic iron oxide nanoparticles (SPIONs) and mannose-coated SPIONs (mSPIONs). Scar bar is 20 nm. (C, D) The average diameter of SPIONs and mSPIONs was calculated from TEM images (histogram in the center). (E) Photograph of bubble production after 30 min incubation of 100 mM H<sub>2</sub>O<sub>2</sub> with 50 µg/mL SPIONs or mSPIONs. (F) H<sub>2</sub>O<sub>2</sub> scavenging assay using terephthalic acid (TA). All data are presented as the mean  $\pm$  SD. One-way ANOVA was used for (F). \*\*\* $P < 0.001$  vs. the TA group; ### $P < 0.001$  vs. the TA + H<sub>2</sub>O<sub>2</sub> group.  $n = 3$  per group.

increased intracellular fluorescence after stimulation with H<sub>2</sub>O<sub>2</sub>, indicating significant H<sub>2</sub>O<sub>2</sub> (Fig. 3B and C) and ROS production (Fig. 3D and E), which were strongly inhibited by SPIONs or mSPIONs pre-treatment (Fig. 3B–E). Consequently, SPIONs and mSPIONs abrogated the cytotoxicity of H<sub>2</sub>O<sub>2</sub> (Figs. S2C and D). These results suggest that SPION and mSPIONs reduce the cellular ROS by their CAT-like activity in the intracellular environment.

### 3.3. mSPIONs reduce the release of pro-inflammatory factors induced by H<sub>2</sub>O<sub>2</sub> in vitro

The inflammatory response has been demonstrated to play a critical role in cognitive decline in POCD [5], and ROS overproduction leads to increased secretion of pro-inflammatory factors (Fig. 4A). Since

demonstrated the H<sub>2</sub>O<sub>2</sub> scavenging ability of mSPIONs, we further studied whether pre-treatment with mSPIONs possessing stronger antioxidant properties could reduce key pro-inflammatory factors triggered by H<sub>2</sub>O<sub>2</sub> in J774A.1 cells. As shown in Fig. 4B and C, H<sub>2</sub>O<sub>2</sub> treatment significantly increased the secretion of IL-1 $\beta$  and TNF- $\alpha$ , which were remarkably reduced by mSPIONs pre-treatment. These data suggest that mSPIONs suppress H<sub>2</sub>O<sub>2</sub>-induced the inflammatory response in vitro. Additionally, the HIF1- $\alpha$ /NF- $\kappa$ B signaling pathway has been widely reported to be involved in the production of pro-inflammatory factors triggered by ROS (Fig. 4A). Indeed, we found that mSPIONs reduced the expression of HIF1- $\alpha$  and p-p65 upregulated by H<sub>2</sub>O<sub>2</sub> (Fig. 4D–F). These results suggest that the HIF1- $\alpha$ /NF- $\kappa$ B signaling pathway may be involved in the inhibition of H<sub>2</sub>O<sub>2</sub>-induced inflammation by mSPIONs.

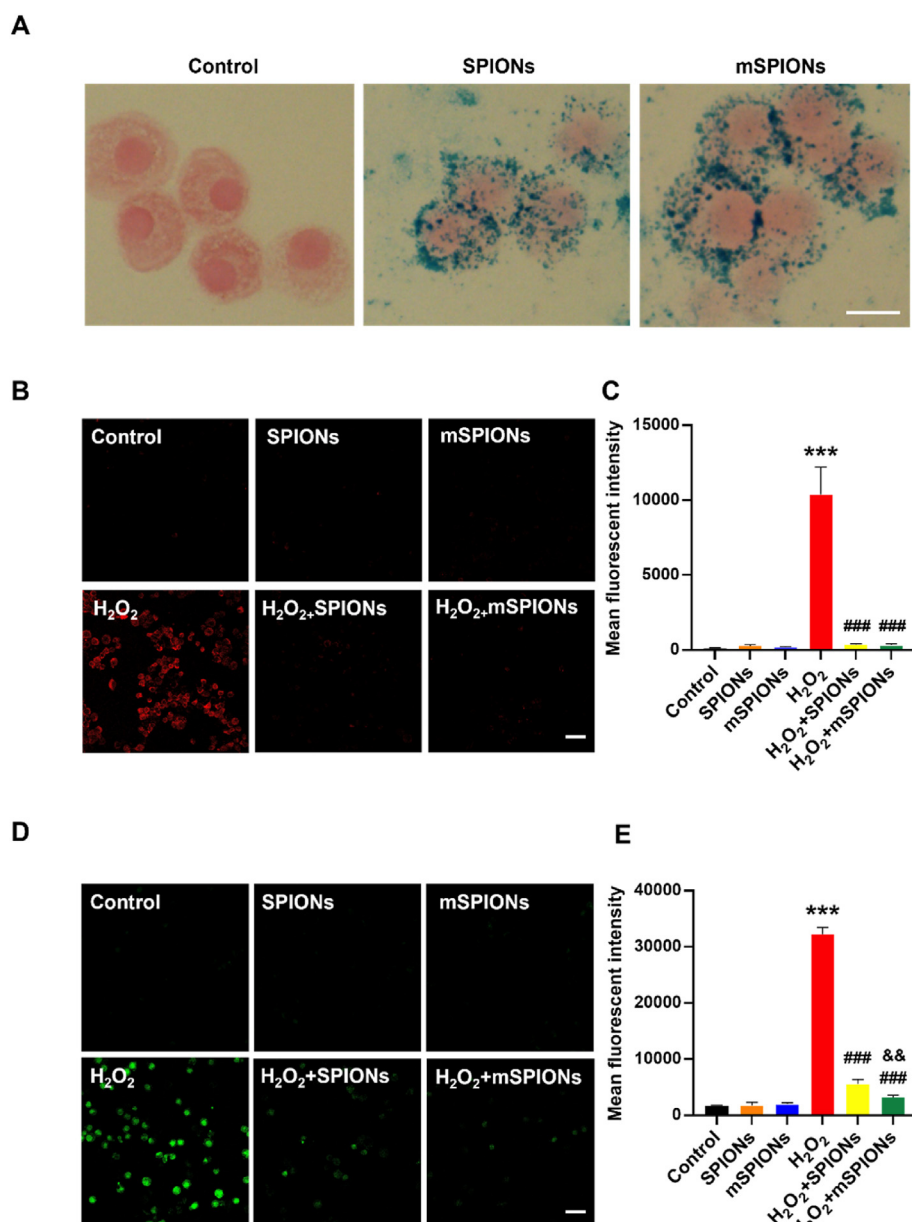


**Fig. 3.** Mannose-coated superparamagnetic iron oxide nanoparticles (mSPIONs) reduce H<sub>2</sub>O<sub>2</sub>-induced ROS generation in J774A.1 cells. (A) Prussian blue staining of J774A.1 cells treated with SPIONs or mSPIONs. Scale bar is 20 μm. (B, C) Representative images and quantification of H<sub>2</sub>O<sub>2</sub> (red) level in J774A.1 cells detected by peroxy orange-1 (PO1). The scale bar is 50 μm. (D, E) Representative images and quantification of ROS (green) levels in J774A.1 cells by staining with 2',7'-dichlorodihydrofluorescein diacetate (DCFH-DA). The scale bar is 50 μm. All data are presented as the mean ± SD. One-way ANOVA was used for (C) and (E). \*\*\*P < 0.001 vs. the control group; ###P < 0.001 vs. the H<sub>2</sub>O<sub>2</sub> group; &&P < 0.01 vs. the H<sub>2</sub>O<sub>2</sub> + SPIONs group. n = 3 per group.

### 3.4. mSPIONs penetrate the blood-brain barrier (BBB)

As mannose can improve the BBB penetration of modified drug [22], we investigated whether mSPIONs can penetrate the BBB in vitro and in vivo. Mouse brain microvascular endothelial cells (bEnd.3) based co-culture system is commonly used to test the BBB penetration of drugs in vitro. As shown in Fig. 5A, the nanoparticles crossed the bEnd.3 layer and were taken up by J774A.1 cells. After the co-culture system was established, we analyzed the Fe content in J774A.1 cells after treatment with mSPIONs or SPIONs in apical medium using ICP-MS (Fig. 5A). The result showed that the Fe content in J774A.1 cells was significantly increased in the mSPIONs group compared to the other groups (Fig. 5B), indicating that mSPIONs has the ability to penetrate the BBB in vitro. And the BBB penetration of mSPIONs may be mediated by GLUT-1, which is a transporter protein on bEnd.3 cells (Fig. 53B). Next, the ICP-MS detection and fluorescent imaging experiments were performed to confirm the BBB penetration ability of mSPIONs in vivo (Fig. 5C). As shown in Fig. 5D, mice that underwent IV injection of mSPIONs had significantly higher Fe content than that in the control group and in the SPIONs group.

Furthermore, BBB penetration of mSPIONs was confirmed using fluorescein isothiocyanate (FITC)-labeling and fluorescence microscopy. As shown in Fig. 5E, FITC-mSPIONs were observed in the hippocampal CA1 region 24 h after IV injection; however, FITC-SPIONs were rarely observed. Moreover, by co-staining with the microglia marker ionized calcium binding adaptor molecule 1 (Iba-1), we found that many FITC signals were co-localized with Iba-1-positive microglia in the CA1 region of FITC-mSPIONs-injected mice (Fig. 5F). Next, we tested the BBB penetration and brain retention of mSPIONs in postoperative mice. The Fe content in whole brain was measured by ICP-MS on postoperative days 0, 1, 3, 7, and 14 after a single IV injection of mSPIONs. The result showed that the Fe content were significantly increased on postoperative days 1 and 3; subsequently, it decreased and returned to basal level on postoperative days 7 and 14 (Fig. 5G). Additionally, the results were confirmed by fluorescent imaging. As shown in Fig. 5H, more FITC-mSPIONs were observed in the CA1 region on postoperative days 1 and 3 compared with those on days 0, 7, and 14. Taken together, these results suggest that mSPIONs can penetrate the BBB, and retain for about 3 days in the postoperative brain after a single IV injection.

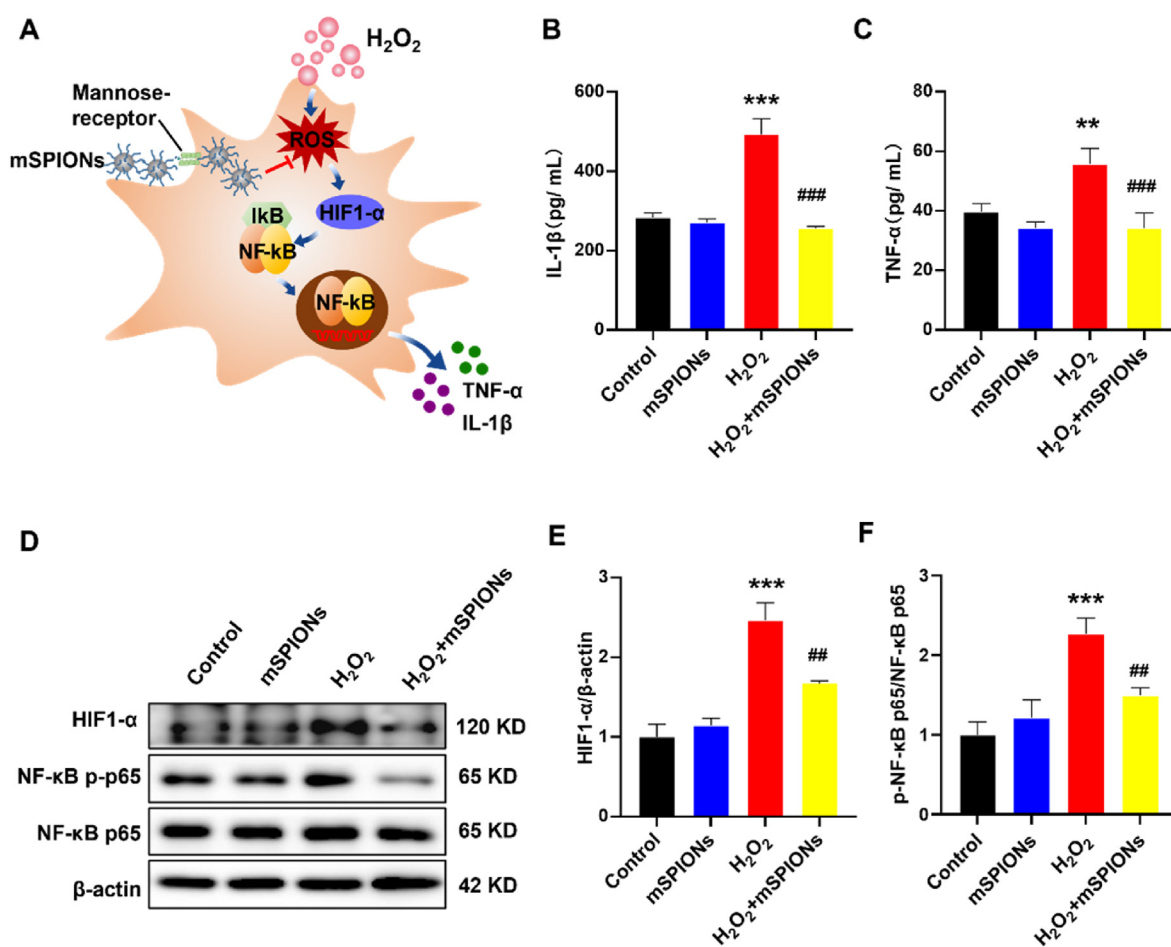


**Fig. 4.** Mannose-coated superparamagnetic iron oxide nanoparticles (mSPIONs) reduce H<sub>2</sub>O<sub>2</sub>-induced pro-inflammatory factors production in J774A.1 cells. (A) Schematic illustration of the signaling pathway for H<sub>2</sub>O<sub>2</sub>-induced production of pro-inflammatory factors. (B, C) The concentrations of IL-1β and TNF-α in J774A.1 cells were measured by ELISA. (D–F) The protein levels of HIF1-α, NF-κB p65, NF-κB p-p65 were assessed by western blot. All data are presented as the mean ± SD. One-way ANOVA was used for (B), (C), (E), and (F). \*\*P < 0.01, \*\*\*P < 0.001 vs. the control group; ##P < 0.01, ###P < 0.001 vs. the H<sub>2</sub>O<sub>2</sub> group. n = 3 per group.

### 3.5. mSPIONs reduce ROS generation and neuroinflammation in postoperative mice hippocampus

Next, the antioxidant activity of the mSPIONs was tested in mice that underwent tibia fracture surgery. Dihydroethidium (DHE) was used to probe ROS in vivo. The mean DHE fluorescence intensity of the hippocampus was significantly increased in mice that underwent surgery compared with the sham-operated mice, while mSPIONs pre-treatment significantly alleviated surgery-elevated fluorescence signals (Fig. 6A). These results confirm the ROS scavenging by mSPIONs. Neuroinflammation plays a critical role in POCD [5], while overproduction of ROS in the hippocampus promotes the secretion of pro-inflammatory factors [7]. Consistently, we found that surgery significantly increased the levels of IL-1β and TNF-α in the hippocampus, whereas mSPIONs remarkably alleviated the surgery-induced upregulation of IL-1β and TNF-α (Fig. 6B and C). Consistent with results in vitro, we found that pre-treatment with mSPIONs reduced the surgery-induced upregulation of HIF1-α and p-p65 expression in the hippocampus (Fig. 6D–F).

### 3.6. mSPIONs improve cognitive impairment after surgery

Subsequently, we assessed whether the alleviation of neuroinflammation by mSPIONs affected the behavior of postoperative mice. The hippocampal-dependent cognitive function was assessed by a novel object recognition (NOR) test and a contextual trace-fear conditioning (TFC) test at 3 days after surgery (Fig. 7A). The NOR test consists of 3

sequential daily trials (Fig. 7B). As shown in Fig. S4A, the total interaction time did not differ within each group during the training phase, indicating that they had the same motivation and interest in the object. During the testing phase, we found that sham-operated mice spent significantly more time interacting with the novel object, indicating a preference for it, whereas surgery abrogated this preference, and surgery mice treated with mSPIONs restored a preference for the novel object (Fig. 7C and D). Then discrimination index (DI) was analyzed to further assess the recognition memory of mice between groups. Consistent with the results for interaction time, the DI was significantly lower in the surgery group than in the sham group, whereas the DI of surgery mice was remarkably increased by mSPIONs treatment (Fig. 7E). These results suggest that mSPIONs treatment improve the cognitive function of mice after surgery. To further assess the cognitive function of postoperative mice, TFC was then utilized in a different cohort of mice. TFC consists of a conditioning session and a contextual test. During the conditioning session, the mice received six pairs of 70-dB sine wave tones and 0.70 mA of electrical foot shock to establish fear memory, and then the mice were returned to the same chamber for the contextual test. When placed back in the original conditioning context, the mice showed freezing as their fear memory was recalled. In contrast, mice with memory impairment were more active, as fear memory would not be evoked, and thus they could detect continuously higher startle amplitude which indicated the locomotor activities of mice (Fig. 7F). Freezing behavior is described as an immobile posture without any movement, except for respiration. During the conditioning session, the baseline freezing % before surgery

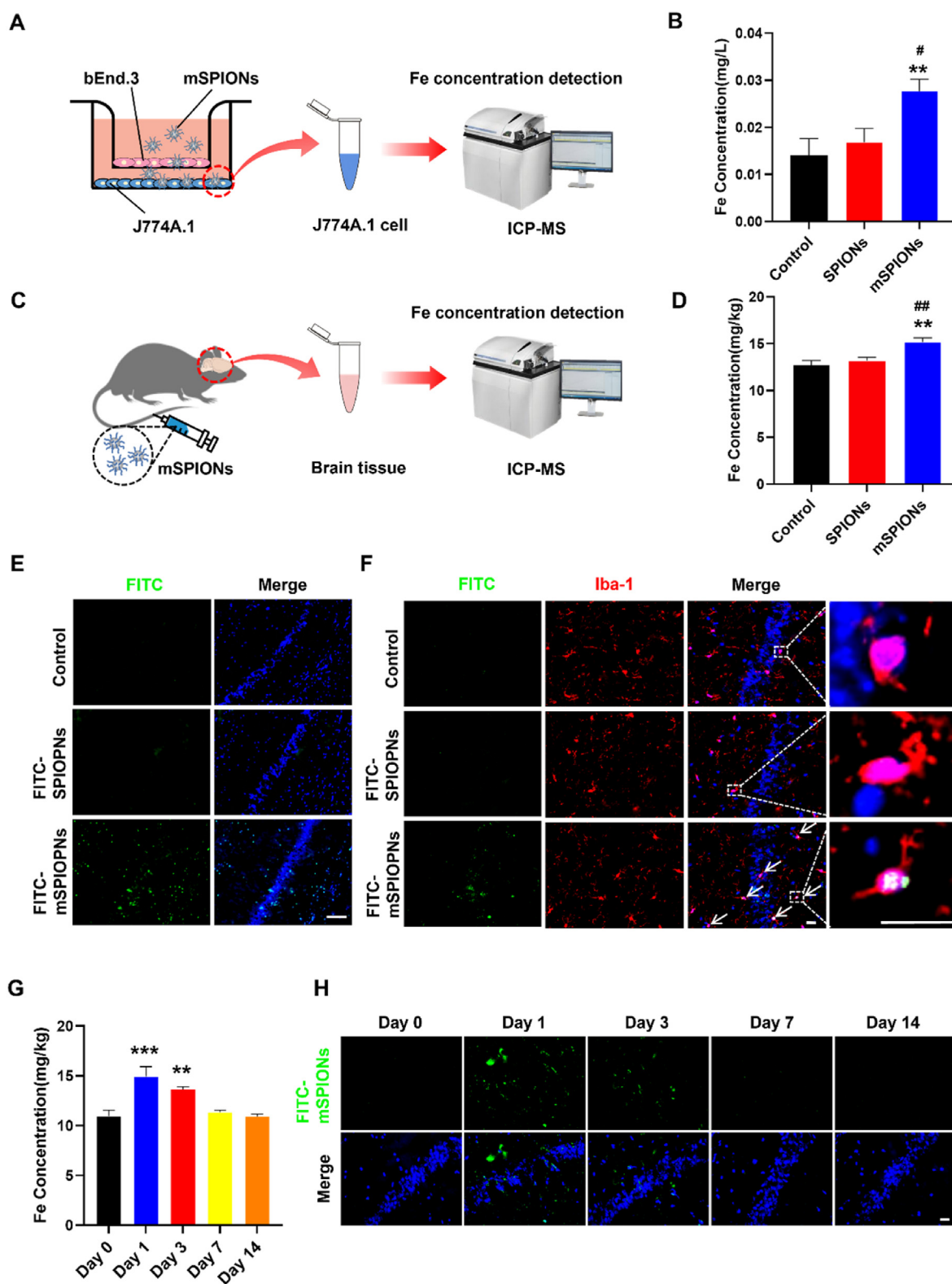


**Fig. 5.** Mannose-coated superparamagnetic iron oxide nanoparticles (mSPIONs) penetrate the blood-brain barrier (BBB). (A) Schematic illustration of BBB model in vitro. The Fe content in J774A.1 cells was measured by inductively coupled plasma mass spectrometry (ICP-MS). (B) ICP-MS analysis of intracellular Fe content. (C) Schematic illustration of the Fe content in whole brain using ICP-MS. (D) ICP-MS analysis of whole brain. (E) Representative fluorescence images of FITC-SPIONs (green) and FITC-mSPIONs (green) in the hippocampal CA1 region. The scale bar is 100  $\mu$ m. (F) Representative fluorescence images of microglia (red) taking up FITC-SPIONs (green) and FITC-mSPIONs (green) in the hippocampal CA1 region. The scale bar is 20  $\mu$ m. (G) ICP-MS analysis of Fe content in whole brain on postoperative days 0, 1, 3, 7, and 14. (H) Representative fluorescence images of FITC-mSPIONs (green) in the hippocampal CA1 region on postoperative days 0, 1, 3, 7, and 14. The scale bar is 20  $\mu$ m. For all graphs, the data are presented as the mean  $\pm$  SD. One-way ANOVA was used for (B), (D), and (G). <sup>\*\*</sup> $P < 0.01$  and <sup>\*\*\*</sup> $P < 0.001$  vs. the control group or the postoperative day 0 group; <sup>#</sup> $P < 0.05$ , <sup>##</sup> $P < 0.01$  vs. the SPIONs group.  $n = 3$  per group.

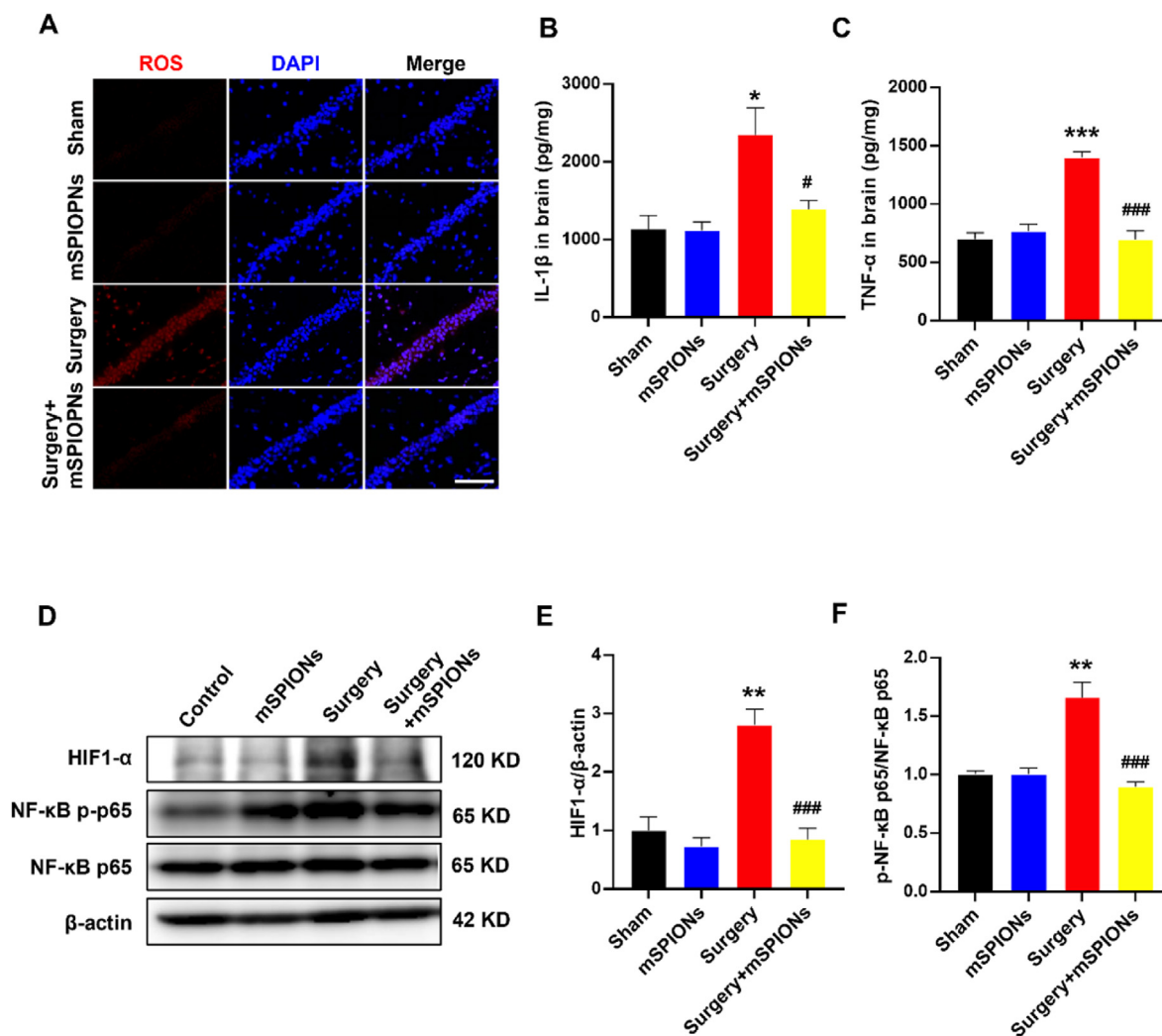


**Fig. 6.** Mannose-coated superparamagnetic iron oxide nanoparticles (mSPIONs) alleviate surgery-induced ROS generation and neuroinflammation. (A) Representative fluorescence staining for ROS (red) in the hippocampal CA1. The scale bar is 100  $\mu$ m. (B, C) The concentrations of IL-1 $\beta$  and TNF- $\alpha$  in hippocampus were measured by ELISA. (D–F) The protein levels of HIF1- $\alpha$ , NF- $\kappa$ B p65 and NF- $\kappa$ B p-p65 were assessed by western blot. All data are presented as the mean  $\pm$  SD. One-way ANOVA was used for (B), (C), (E), and (F). \* $P < 0.05$ , \*\* $P < 0.01$  and \*\*\* $P < 0.001$  vs. the sham group; # $P < 0.05$ , ### $P < 0.001$  vs. the surgery group.  $n = 3$  per group.

was calculated, and there was no significant difference in the baseline freezing % among the groups (Fig. S4B). However, mice that underwent surgery displayed more active than sham-operated mice on postoperative day 3, while mSPIONs-treated mice exhibited increased freezing behavior compared with those in the surgery group, suggesting that mSPIONs attenuated surgery-induced fear memory impairment (Fig. 7G). The statistical result also showed that mSPIONs were able to recover the surgery-induced reduction in freezing time to a degree that did not differ from that of the sham-operated mice (Fig. 7H). These results indicate that mSPIONs prevent surgery-induced hippocampus-dependent memory impairment. Notably, mSPIONs administration did not induce evident pathological changes in major organs at this dose (Fig. S5).

#### 4. Discussion

In the present study we evaluated the effects of mSPIONs on ROS production and inflammatory response to H<sub>2</sub>O<sub>2</sub> treatment in vitro and in surgical models, as well as the mechanisms that may be involved. Our results suggest that mSPIONs exhibit favorable CAT-like activity in vivo and in vitro, thereby reducing surgery-induced ROS and pro-inflammatory factor production to prevent cognitive impairment. Furthermore, we reveal that the underlying mechanisms involved downregulation of the HIF1- $\alpha$ /NF- $\kappa$ B signaling pathway.

POCD is a common postoperative morbidity that poses a serious threat to the quality of life of patients, especially the elderly population. The optimal treatment for POCD currently focuses on the prevention, early identification, and management of potential perioperative risk factors. Several drugs targeting neuroinflammation and oxidative stress have been studied in clinical trials but have failed to achieve satisfactory results. Dexamethasone was reported to reduce the incidence of POCD in patients undergoing cardiac surgery on the 6th day and 4 years after surgery but did not improve long-term cognitive function in patients [29]. A small randomized controlled trial reported that preoperative statin therapy attenuated the early postoperative memory impairment in patients undergoing off-pump coronary artery bypass (OPCAB) surgery [30]. However, statins may also be associated with acute memory deficits [31]. Thus, new treatments are urgently needed to alleviate the socio-economic burden of POCD.

Nanotechnology may be a promising strategy for the treatment of CNS diseases. Currently, magnetic nanoparticles are one of the most widely studied nanomaterials. They provide various advantages and opportunities in biomedical applications. Several IONPs are approved by the U.S. Food and Drug Administration (FDA) for clinical use to date including magnetic resonance imaging (MRI), oral gastrointestinal tract imaging agent, iron deficiency, and tumor therapy [16,32], indicating their favorable biosafety. In addition, studies on the intrinsic structure,

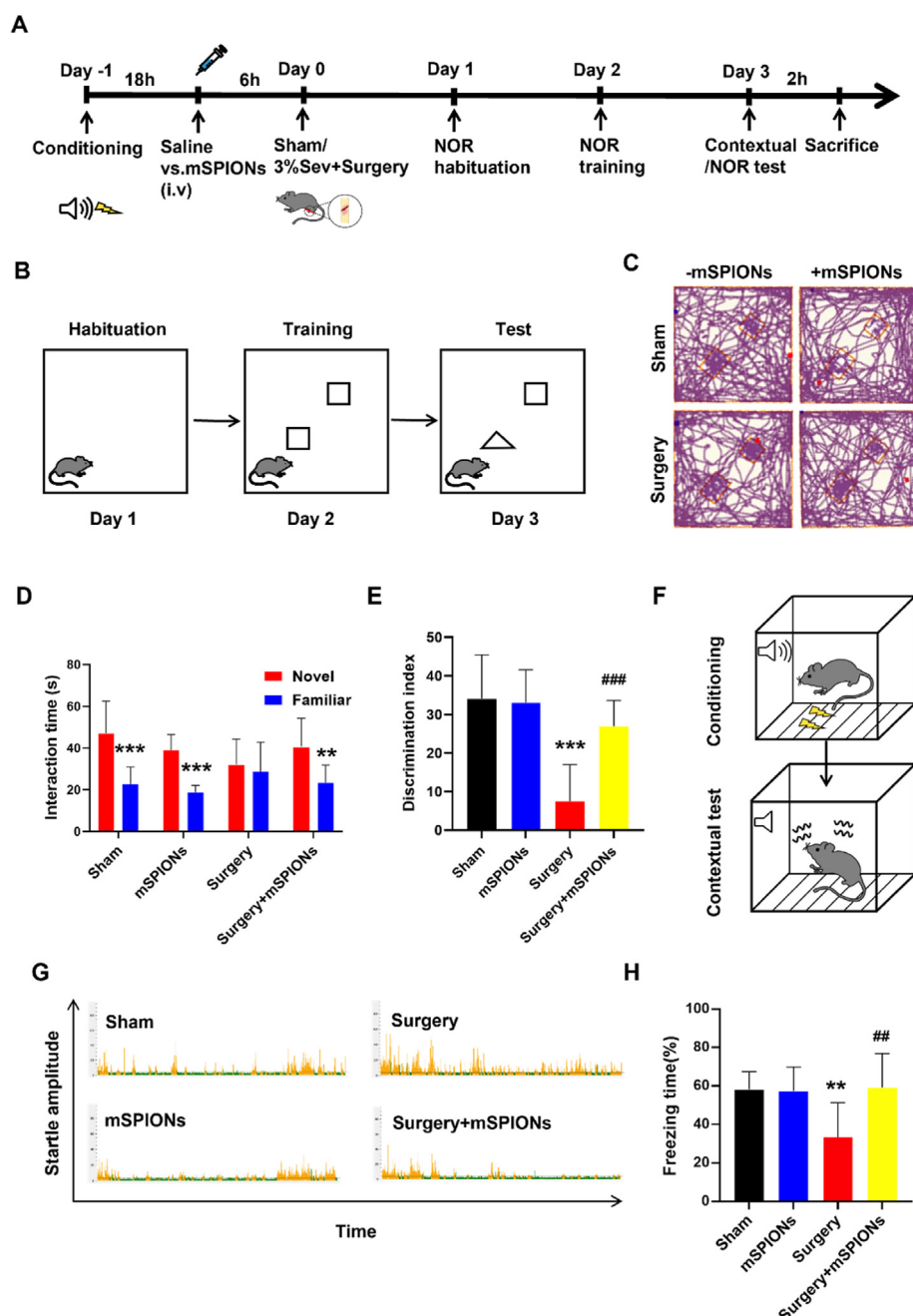


**Fig. 7.** Mannose-coated superparamagnetic iron oxide nanoparticles (mSPIONs) prevent surgery-induced cognitive dysfunction. (A) Schematic timeline of the experimental procedure. (B) Schematic diagram of novel object recognition (NOR). (C) Representative movement tracks in the testing phase of NOR. (D, E) The time spent interacting with novel object and discrimination index (DI) in the NOR, respectively. (F) Schematic diagram of trace-fear conditioning (TFC). (G) Representative images of changes in startle amplitude of mice. (H) The percentage of freezing time in the contextual tests. All data are presented as the mean  $\pm$  SD. Two-way ANOVA was used for (D). One-way ANOVA was used for (E) and (H). \*\* $P < 0.01$ , \*\*\* $P < 0.001$  vs. the sham group or the novel group; ## $P < 0.01$ , ### $P < 0.001$  vs. the surgery group.  $n = 10$  per group.

magnetic properties, and biological effects of IONPs are driving new biomedical applications in magnetic hyperthermia, drug delivery, and brain diseases [33]. Zhang et al. found that dietary IONPs exhibited CAT-like activity in vivo, which can scavenge ROS and ameliorate neurodegeneration in *Drosophila* [19]. Chung et al. found that dextran-coated IONPs (Dex-IONPs)-labeled human mesenchymal stem cell transplantation improved functional recovery efficacy in Parkinson's disease mice and rescued the loss of dopaminergic (DA) neurons [34]. Sanati et al. showed that PEG-modified SPIONs significantly limited spatial memory impairment and neuronal oxidative damage in AD mice [35]. Collectively, IONPs have shown great advantages and potential in biomedical applications. Based on these findings, we synthesized mSPIONs with an average diameter of approximately 11 nm and a favorable biocompatibility. SPIONs and mSPIONs at a concentration of 50  $\mu\text{g}/\text{ml}$  showed similar toxicity to J774A.1 cells. In contrast, previous study has shown that bare IONPs are more cytotoxic than coated

nanoparticles [36], and this difference may be related to the different shapes, sizes, surface coatings, types of cells, and processing times of IONPs [37]. Moreover, the distribution and intracellular microenvironment of IONPs are key factors that affect their cytotoxicity. IONPs react with  $\text{H}_2\text{O}_2$  through the Fenton reaction to produce hydroxyl radicals; however, this reaction is strongly dependent on pH. The cells death was induced by highly cytotoxic hydroxyl radicals generated through peroxidase-catalyzed  $\text{H}_2\text{O}_2$  when IONPs were internalized into cells and trapped in acidic lysosomes [38]. In contrast, in a neutral cytoplasmic environment, IONPs preferentially exhibit CAT-like activity, and  $\text{H}_2\text{O}_2$  is decomposed into nontoxic species, protecting cells from oxidative stress [39]. The neuroprotective effects of IONPs as  $\text{H}_2\text{O}_2$  scavengers in ischemic stroke have been recently investigated [20,21]. In agreement with previous findings [18], our results confirmed the CAT-like activity of IONPs in a neutral environment through the production of oxygen (a product of  $\text{H}_2\text{O}_2$  decomposition) and experiment with TA.

H<sub>2</sub>O<sub>2</sub> is an extremely toxic ROS that can easily penetrate the plasma membrane and affect neighboring cells, thereby altering intracellular ROS levels. Elevated ROS levels activate microglia and promote the secretion of pro-inflammatory factors [7]. In the present study, we found that mSPIONs reduced the H<sub>2</sub>O<sub>2</sub>-induced increases in ROS and pro-inflammatory factors in the cells and postoperative hippocampus through CAT-like activity. SPIONs and mSPIONs did not show significant differences in H<sub>2</sub>O<sub>2</sub> scavenging, whereas mSPIONs exhibited a stronger ROS-scavenging effect, suggesting that other mechanisms may be involved in IONPs-mediated antioxidant effects. IONPs have also been reported to have anti-inflammatory effects by regulating NF-κB and caveolin-1 (Cav1)-Notch1/HES1, toll-like receptors-4 (TLRs-4), mammalian target of rapamycin (mTOR), and other signaling pathways as well as downregulating ROS production-related enzymes to protect against different disease models [40–45]. Notably, internalized IONPs may increase intracellular ROS levels through the Fenton reaction, but this usually occurs in acidic tumor tissue [46]. Activation of systemic immune responses is an important cause for surgery-induced neuroinflammation. Suppression of systemic inflammation may mitigate the neuroinflammatory effects of surgery [5]. In this study, intravenous injection of mannose-encapsulated SPIONs targeted not only macrophages in the CNS but also in the periphery. Intraperitoneal injection of a mannosylated-polymeric-albumin-manganese dioxide (mSPAM) nano-assembly attenuated LPS-induced secretion of TNF-α and IL-6 in serum and pro-inflammatory proteins expression [24]. Therefore, it is unclear whether peripheral mechanisms are involved in the central anti-inflammatory effects of mSPIONs.

Nuclear factor kappa B (NF-κB) is a core transcription factor that regulates immune and inflammatory processes and is regulated by many factors, including ROS [47]. An inflammatory environment is usually accompanied by hypoxia. Hypoxia-inducible factor-1α (HIF-1α) is an oxygen-sensitive transcription factor that is normally induced under hypoxic conditions [48]. Extensive crosstalk between the two main molecular players involved, HIF-1α (hypoxia) and NF-κB (inflammation), has been reported [49]. We found that mSPIONs reversed the H<sub>2</sub>O<sub>2</sub>-induced increase in HIF-1α and p-p65 expression. However, total p65 expression remained constant. We also observed this effect in mice. Consistent with our results, inhibition of HIF-1α and NF-κB signaling by IONPs has been reported in other studies. Maryam et al. found that SPIONs-labeled human amniotic membrane-derived mesenchymal stem cells (hAMSCs) decreased the number of NF-κB-positive cells after isoproterenol induction [50]. The encapsulated magnetic IONPs (eSPIONs) constructed by Zhang et al. exhibited enhanced CAT-like activity in the presence of an alternating magnetic field, resulting in the inhibition of tumor angiogenesis with a decrease in HIF-1α expression in A549 tumor cells [51]. However, the specific mechanism underlying the regulation of the HIF-1α/NF-κB signaling pathway by IONPs needs to be further explored.

Most drug/gene delivery candidates for CNS disorders fail because they cannot traverse the BBB. Mannose, a specific substrate for glucose transporter protein -1 (GLUT-1), is used as a brain-targeting ligand that allows transporter protein-mediated endocytosis of BBB [22]. GLUT-1 is abundantly expressed in the brain, but it is either absent or below the limit of detection in many normal human tissues. Thus, it can potentially exhibit minimal off-target effects, leading to selective accumulation in the brain [52]. Similarly, studies *in vivo* have confirmed that mSPIONs have the capacity to enhance the effect across the BBB, resulting in approximately 1.5-fold higher Fe content in the brain than baseline levels. More importantly, activated microglia serve as therapeutic targets, and mSPIONs can be phagocytosed by them in the hippocampus owing to their surface mannose receptors and phagocytic properties. However, we did not further assess whether neurons and astrocytes in the hippocampus have taken up of mSPIONs, which may reduce the targeting effect of mSPIONs and cause other effects. In addition, histopathological analyses performed on all vital tissues showed no significant hyperemia, necrosis, or inflammation in any organs. This finding indicates a

favorable safety profile of the mSPIONs and supports a possibility of successful translation to clinical application in the future.

The TFC test, including contextual and cued fear conditioning test, is commonly used method to assess memory capacity in rodents [53]. Specifically, the contextual test is usually used for hippocampus-dependent memory testing, while the cued test is usually used to assess the non-hippocampus-dependent memory, such as amygdala- and cortex-related memory [27,54,55]. A few days after surgery, the TFC memory in rodents correlated well with performance in the Morris water maze [56]. Notably, the retrograde conditioning paradigm (conditioning occurred before surgery) allowed the mice to correctly sample and encode the environment during acquisition. In the present study we observed that young adult mice showed memory loss 3 days after fracture surgery, confirming that surgery disrupts the recall of TFC memory formed in the hippocampus after conditioning. This is consistent with previous evidence of hippocampus dependent cognitive decline in POCD [5]. IONPs have shown improved effects on the performance of a murine model of ischemic stroke in the Y-maze and neurological function tests [20,21]. Our results showed that perioperative mSPIONs treatment improved memory impairment by decreasing ROS production and neuroinflammation.

Our study has several limitations that should be considered. First, we did not detect ROS and inflammation levels in other brain regions to reflect the overall oxidative stress and inflammation status of the postoperative brain. Second, in the current study, we focused only on early postoperative cognitive function; therefore, the development of long-term postoperative cognitive function should be further investigated. Third, we lacked a long-term assessment of the biosafety of mSPIONs as well as quantitative analysis and real-time tracking of the distribution and metabolism of mSPIONs in the brain. Finally, only male mice were used in this study to reduce the effects that estrogen and progesterin concentrations exert on learning and memory in female mice. Therefore, the effects of mSPIONs on postoperative female mice remain unknown. These limitations suggest the need for further investigations.

## 5. Conclusion

In conclusion, the mSPIONs nanozyme with CAT-like activity were found to scavenge ROS and reduce inflammation levels *in vitro* and in the hippocampus of postoperative mice. Furthermore, mSPIONs administration significantly improved surgery-induced cognitive impairment in mice. The HIF1-α/NF-κB signaling pathway may be involved in the attenuating effects of mSPIONs on inflammation and oxidative stress. This study provides a new approach for preventing POCD using a nanozyme.

## Credit author statement

Q.Z.: Performed experiments, Data analysis & Writing. Y.H.: Performed experiments, Data analysis & Writing. X.Z.: Performed cytology-related experiments, Data analysis & Writing. L.P.: Performed cytology-related experiments, Data analysis & Writing. H.W.: Performed data analysis, Funding, & Writing. S.G.: Performed writing-review & Editing. Z.Y.: Conceptualization, Writing-review & Editing. J.Z.: Conceptualization, Funding, Writing-review & Editing. X.L.: Conceptualization, Funding, Writing-review & Editing.

## Declaration of competing interest

The authors declare that they have no known competing financial interests or personal relationships that could have appeared to influence the work reported in this paper.

## Data availability

Data will be made available on request.

## Acknowledgments

We thank Key Laboratory of Anesthesiology and Perioperative Medicine of Anhui Higher Education Institutes for technical support. This work was supported by the National Natural Science Foundation of China (Beijing, China) grant Nos. 82171192 (to Dr. Liu) and 82271217 (to Dr. Zhang), the Natural Science Research Project of Anhui (Hefei, Anhui) Universities grant No. KJ2020A0178 (to Dr. Wang).

## Appendix A. Supplementary data

Supplementary data to this article can be found online at <https://doi.org/10.1016/j.mtbio.2023.100568>.

## References

- Evered, B. Silbert, D.S. Knopman, D.A. Scott, S.T. DeKosky, L.S. Rasmussen, E.S. Oh, G. Crosby, M. Berger, R.G. Eckenhoff, G. Nomenclature Consensus Working, Recommendations for the nomenclature of cognitive change associated with anaesthesia and surgery-2018, *Br. J. Anaesth.* 121 (2018) 1005–1012.
- K.J. Hogan, L.C. Bratzke, K.L. Hogan, Informed consent and cognitive dysfunction after noncardiac surgery in the elderly, *Anesth. Analg.* 126 (2018) 629–631.
- V. Fodale, L.B. Santamaria, D. Schifilliti, P.K. Mandal, Anaesthetics and postoperative cognitive dysfunction: a pathological mechanism mimicking Alzheimer's disease, *Anaesthesia* 65 (2010) 388–395.
- M.B. Netto, A.N. de Oliveira Junior, M. Goldim, K. Mathias, M.E. Fileti, N. da Rosa, A.O. Laurentino, B.X. de Farias, A.B. Costa, G.T. Rezin, J.J. Fortunato, A.D. Giustina, T. Barichello, F. Dal-Pizzol, F. Petronilho, Oxidative stress and mitochondrial dysfunction contributes to postoperative cognitive dysfunction in elderly rats, *Brain Behav. Immun.* 73 (2018) 661–669.
- M. Cibelli, A.R. Fidalgo, N. Terrando, D. Ma, C. Monaco, M. Feldmann, M. Takata, I.J. Lever, J. Nanchahal, M.S. Fanselow, M. Maze, Role of interleukin-1beta in postoperative cognitive dysfunction, *Ann. Neurol.* 68 (2010) 360–368.
- L.L. Qiu, D. Luo, H. Zhang, Y.S. Shi, Y.J. Li, D. Wu, J. Chen, M.H. Ji, J.J. Yang, Nox-2-Mediated phenotype loss of hippocampal parvalbumin interneurons might contribute to postoperative cognitive decline in aging mice, *Front. Aging Neurosci.* 8 (2016) 234.
- L.L. Qiu, M.H. Ji, H. Zhang, J.J. Yang, X.R. Sun, H. Tang, J. Wang, W.X. Liu, J.J. Yang, NADPH oxidase 2-derived reactive oxygen species in the hippocampus might contribute to microglial activation in postoperative cognitive dysfunction in aged mice, *Brain Behav. Immun.* 51 (2016) 109–118.
- Y. Huang, J. Ren, X. Qu, Nanozymes: classification, catalytic mechanisms, activity regulation, and applications, *Chem. Rev.* 119 (2019) 4357–4412.
- Y. Chen, L. Liu, Modern methods for delivery of drugs across the blood-brain barrier, *Adv. Drug Deliv. Rev.* 64 (2012) 640–665.
- Y. Cao, Z. Li, H. Li, C. Ni, L. Li, N. Yang, C. Shi, Y. Zhong, D. Cui, X. Guo, Hypoxia-inducible factor-1alpha is involved in isoflurane-induced blood-brain barrier disruption in aged rats model of POCD, *Behav. Brain Res.* 339 (2018) 39–46.
- N. Hu, C. Wang, Y. Zheng, J. Ao, C. Zhang, K. Xie, Y. Li, H. Wang, Y. Yu, G. Wang, The role of the Wnt/beta-catenin-Annexin A1 pathway in the process of sevoflurane-induced cognitive dysfunction, *J. Neurochem.* 137 (2016) 240–252.
- Z. Cheng, J. Zhang, H. Liu, Y. Li, Y. Zhao, E. Yang, Central nervous system penetration for small molecule therapeutic agents does not increase in multiple sclerosis- and Alzheimer's disease-related animal models despite reported blood-brain barrier disruption, *Drug Metab. Dispos.* 38 (2010) 1355–1361.
- X. Shan, X. Gong, J. Li, J. Wen, Y. Li, Z. Zhang, Current approaches of nanomedicines in the market and various stage of clinical translation, *Acta Pharm. Sin.* B 12 (2022) 3028–3048.
- A.D. Maynard, Don't define nanomaterials, *Nature* 475 (2011) 31.
- B. Unnikrishnan, C.W. Lien, H.W. Chu, C.C. Huang, A review on metal nanozyme-based sensing of heavy metal ions: challenges and future perspectives, *J. Hazard Mater.* 401 (2021), 123397.
- S.M. Dadfar, K. Roemhild, N.I. Drude, S. von Stillfried, R. Knuchel, F. Kiessling, T. Lammers, Iron oxide nanoparticles: diagnostic, therapeutic and theranostic applications, *Adv. Drug Deliv. Rev.* 138 (2019) 302–325.
- L. Gao, J. Zhuang, L. Nie, J. Zhang, Y. Zhang, N. Gu, T. Wang, J. Feng, D. Yang, S. Perrett, X. Yan, Intrinsic peroxidase-like activity of ferromagnetic nanoparticles, *Nat. Nanotechnol.* 2 (2007) 577–583.
- Z. Chen, J.J. Yin, Y.T. Zhou, Y. Zhang, L. Song, M. Song, S. Hu, N. Gu, Dual enzyme-like activities of iron oxide nanoparticles and their implication for diminishing cytotoxicity, *ACS Nano* 6 (2012) 4001–4012.
- Y. Zhang, Z. Wang, X. Li, L. Wang, M. Yin, L. Wang, N. Chen, C. Fan, H. Song, Dietary iron oxide nanoparticles delay aging and ameliorate neurodegeneration in *Drosophila*, *Adv. Mater.* 28 (2016) 1387–1393.
- B.C. Yan, J. Cao, J. Liu, Y. Gu, Z. Xu, D. Li, L. Gao, Dietary Fe3O4 nanozymes prevent the injury of neurons and blood-brain barrier integrity from cerebral ischemic stroke, *ACS Biomater. Sci. Eng.* 7 (2021) 299–310.
- Y. Liu, X. Wang, X. Li, S. Qiao, G. Huang, D.M. Hermann, T.R. Doepfner, M. Zeng, W. Liu, G. Xu, L. Ren, Y. Zhang, W. Liu, E. Casals, W. Li, Y.C. Wang, A Co-doped Fe3O4 nanozyme shows enhanced reactive oxygen and nitrogen species scavenging activity and ameliorates the deleterious effects of ischemic stroke, *ACS Appl. Mater. Interfaces* 13 (2021) 46213–46224.
- P. Zhao, Y. Wang, X. Kang, A. Wu, W. Yin, Y. Tang, J. Wang, M. Zhang, Y. Duan, Y. Huang, Dual-targeting biomimetic delivery for anti-glioma activity via remodeling the tumor microenvironment and directing macrophage-mediated immunotherapy, *Chem. Sci.* 9 (2018) 2674–2689.
- H. Vu-Quang, M.K. Yoo, H.J. Jeong, H.J. Lee, M. Muthiah, J.H. Rhee, J.H. Lee, C.S. Cho, Y.Y. Jeong, I.K. Park, Targeted delivery of mannan-coated superparamagnetic iron oxide nanoparticles to antigen-presenting cells for magnetic resonance-based diagnosis of metastatic lymph nodes in vivo, *Acta Biomater.* 7 (2011) 3935–3945.
- S.K. Rajendrakumar, V. Revuri, M. Samidurai, A. Mohapatra, J.H. Lee, P. Ganesan, J. Jo, Y.K. Lee, I.K. Park, Peroxidase-Mimicking nanoassembly mitigates lipopolysaccharide-induced endotoxemia and cognitive damage in the brain by impeding inflammatory signaling in macrophages, *Nano Lett.* 18 (2018) 6417–6426.
- R. Liu, J. Yang, L. Liu, Z. Lu, Z. Shi, W. Ji, J. Shen, X. Zhang, An "Amyloid-beta cleaner" for the treatment of Alzheimer's disease by normalizing microglial dysfunction, *Adv. Sci.* 7 (2020), 1901555.
- X. Feng, M. Valdearcos, Y. Uchida, D. Lutrin, M. Maze, S.K. Koliwad, Microglia mediate postoperative hippocampal inflammation and cognitive decline in mice, *JCI Insight* 2 (2017), e91229.
- L. Sun, R. Dong, X. Xu, X. Yang, M. Peng, Activation of cannabinoid receptor type 2 attenuates surgery-induced cognitive impairment in mice through anti-inflammatory activity, *J. Neuroinflammation* 14 (2017) 138.
- T. Finkel, N.J. Holbrook, Oxidants, Oxidative stress and the biology of ageing, *Nature* 408 (2000) 239–247.
- S. Glumac, G. Kardum, L. Sodic, C. Bulat, I. Covic, M. Carev, N. Karanovic, Longitudinal assessment of preoperative dexamethasone administration on cognitive function after cardiac surgery: a 4-year follow-up of a randomized controlled trial, *BMC Anesthesiol.* 21 (2021) 129.
- S. Das, S.K. Nanda, A.K. Bisoi, A.N. Wadhawan, Effect of preoperative statin therapy on early postoperative memory impairment after off-pump coronary artery bypass surgery, *Ann. Card Anaesth.* 19 (2016) 38–44.
- M.A. Evans, B.A. Golomb, Statin-associated adverse cognitive effects: survey results from 171 patients, *Pharmacotherapy* 29 (2009) 800–811.
- Y. Huang, J.C. Hsu, H. Koo, D.P. Cormode, Repurposing ferumoxytol: diagnostic and therapeutic applications of an FDA-approved nanoparticle, *Theranostics* 12 (2022) 796–816.
- Z. Mao, X. Li, P. Wang, H. Yan, Iron oxide nanoparticles for biomedical applications: an updated patent review (2015–2021), *Expert Opin. Ther. Pat.* 32 (2022) 939–952.
- T.H. Chung, S.C. Hsu, S.H. Wu, J.K. Hsiao, C.P. Lin, M. Yao, D.M. Huang, Dextran-coated iron oxide nanoparticle-improved therapeutic effects of human mesenchymal stem cells in a mouse model of Parkinson's disease, *Nanoscale* 10 (2018) 2998–3007.
- M. Sanati, S. Aminyavari, F. Khodagholi, M.J. Hajipour, P. Sadeghi, M. Noruzi, A. Moshtagh, H. Behmadi, M. Sharifzadeh, PEGylated superparamagnetic iron oxide nanoparticles (SPIONs) ameliorate learning and memory deficit in a rat model of Alzheimer's disease: potential participation of STIMs, *Neurotoxicology* 85 (2021) 145–159.
- S. Shukla, A. Jadaun, V. Arora, R.K. Sinha, N. Biyani, V.K. Jain, In vitro toxicity assessment of chitosan oligosaccharide coated iron oxide nanoparticles, *Toxicol Rep* 2 (2015) 27–39.
- I.M. Adjei, B. Sharma, V. Labhasetwar, Nanoparticles: cellular uptake and cytotoxicity, *Adv. Exp. Med. Biol.* 811 (2014) 73–91.
- Y. Liu, P.C. Naha, G. Hwang, D. Kim, Y. Huang, A. Simon-Soro, H.I. Jung, Z. Ren, Y. Li, S. Gubara, F. Alawi, D. Zero, A.T. Hara, D.P. Cormode, H. Koo, Topical ferumoxytol nanoparticles disrupt biofilms and prevent tooth decay in vivo via intrinsic catalytic activity, *Nat. Commun.* 9 (2018) 2920.
- B. Yang, Y. Chen, J. Shi, Reactive oxygen species (ROS)-Based nanomedicine, *Chem. Rev.* 119 (2019) 4881–4985.
- Y. Pan, J. Li, X. Xia, J. Wang, Q. Jiang, J. Yang, H. Dou, H. Liang, K. Li, Y. Hou, beta-galactan-coupled superparamagnetic iron oxide nanoparticles induce trained immunity to protect mice against sepsis, *Theranostics* 12 (2022) 675–688.
- Y. Chen, Q. Zhang, X. Qin, J. Li, Y. Zhao, Y. Xia, Superparamagnetic iron oxide nanoparticles protect human gingival fibroblasts from porphyromonas gingivalis invasion and inflammatory stimulation, *Int. J. Nanomed.* 17 (2022) 45–60.
- K. Marycz, P. Sobierajska, M. Roecken, K. Kornicka-Garbowska, M. Kepska, R. Idczak, J.M. Nedelec, R.J. Wluzus, Iron oxides nanoparticles (IOs) exposed to magnetic field promote expression of osteogenic markers in osteoblasts through integrin alpha-3 (INTA-3) activation, inhibits osteoclasts activity and exerts anti-inflammatory action, *J. Nanobiotechnol.* 18 (2020) 33.
- Y. Chen, Z. Zeng, H. Ying, C. Wu, S. Chen, Superparamagnetic iron oxide nanoparticles attenuate lipopolysaccharide-induced inflammatory responses through modulation of toll-like receptor 4 expression, *J. Appl. Toxicol.* 40 (2020) 1067–1075.
- Y. Xu, Y. Li, X. Liu, Y. Pan, Z. Sun, Y. Xue, T. Wang, H. Dou, Y. Hou, SPIONs enhances IL-10-producing macrophages to relieve sepsis via Cav1-Notch1/HES1-mediated autophagy, *Int. J. Nanomed.* 14 (2019) 6779–6797.
- S. Grosse, J. Stenvik, A.M. Nilsen, Iron oxide nanoparticles modulate lipopolysaccharide-induced inflammatory responses in primary human monocytes, *Int. J. Nanomed.* 11 (2016) 4625–4642.
- S. Bai, N. Yang, X. Wang, F. Gong, Z. Dong, Y. Gong, Z. Liu, L. Cheng, Ultrasmall iron-doped titanium oxide nanodots for enhanced sonodynamic and chemodynamic cancer therapy, *ACS Nano* 14 (2020) 15119–15130.

- [47] M.J. Morgan, Z.G. Liu, Crosstalk of reactive oxygen species and NF-kappaB signaling, *Cell Res.* 21 (2011) 103–115.
- [48] G.L. Semenza, Hypoxia-inducible factors in physiology and medicine, *Cell* 148 (2012) 399–408.
- [49] D. Bandarra, J. Biddlestone, S. Mudie, H.A. Muller, S. Rocha, HIF-1alpha restricts NF-kappaB-dependent gene expression to control innate immunity signals, *Dis Model Mech* 8 (2015) 169–181.
- [50] M. Naseroleslami, N. Aboutaleb, B. Mokhtari, Amniotic membrane mesenchymal stem cells labeled by iron oxide nanoparticles exert cardioprotective effects against isoproterenol (ISO)-induced myocardial damage by targeting inflammatory MAPK/NF-kappaB pathway, *Drug Deliv Transl Res* 11 (2021) 242–254.
- [51] Y. Zhang, X. Wang, C. Chu, Z. Zhou, B. Chen, X. Pang, G. Lin, H. Lin, Y. Guo, E. Ren, P. Lv, Y. Shi, Q. Zheng, X. Yan, X. Chen, G. Liu, Genetically engineered magnetic nanocages for cancer magneto-catalytic theranostics, *Nat. Commun.* 11 (2020) 5421.
- [52] A. Godoy, V. Ulloa, F. Rodriguez, K. Reinicke, A.J. Yanez, L. Garcia Mde, R.A. Medina, M. Carrasco, S. Barberis, T. Castro, F. Martinez, X. Koch, J.C. Vera, M.T. Poblete, C.D. Figueroa, B. Peruzzo, F. Perez, F. Nualart, Differential subcellular distribution of glucose transporters GLUT1-6 and GLUT9 in human cancer: ultrastructural localization of GLUT1 and GLUT5 in breast tumor tissues, *J. Cell. Physiol.* 207 (2006) 614–627.
- [53] G.E. Schafe, K. Nader, H.T. Blair, J.E. LeDoux, Memory consolidation of Pavlovian fear conditioning: a cellular and molecular perspective, *Trends Neurosci.* 24 (2001) 540–546.
- [54] H.C. Bergstrom, The neurocircuitry of remote cued fear memory, *Neurosci. Biobehav. Rev.* 71 (2016) 409–417.
- [55] C.S.W. Lai, A. Adler, W.B. Gan, Fear extinction reverses dendritic spine formation induced by fear conditioning in the mouse auditory cortex, *Proc. Natl. Acad. Sci. U. S. A.* 115 (2018) 9306–9311.
- [56] X. Feng, V. Degos, L.G. Koch, S.L. Britton, Y. Zhu, S. Vacas, N. Terrando, J. Nelson, X. Su, M. Maze, Surgery results in exaggerated and persistent cognitive decline in a rat model of the Metabolic Syndrome, *Anesthesiology* 118 (2013) 1098–1105.